Article

Surface optimization governs the local design of physical networks

https://doi.org/10.1038/s41586-025-09784-4

Received: 19 November 2024

Accepted: 21 October 2025

Published online: 7 January 2026

Open access

Check for updates

Xiangyi Meng[1,2,3,4], Benjamin Piazza[3,4], Csaba Both[3,4], Baruch Barzel[3,4,5,6] & Albert-László Barabási[3,4,7,8] ✉

The brain's connectome[1–3] and the vascular system[4] are examples of physical networks whose tangible nature influences their structure, layout and, ultimately, their function. The material resources required to build and maintain these networks have inspired decades of research into wiring economy, offering testable predictions about their expected architecture and organization. Here we empirically explore the local branching geometry of a wide range of physical networks, uncovering systematic violations of the long-standing predictions of wiring minimization. This leads to the hypothesis that predicting the true material cost of physical networks requires us to account for their full three-dimensional geometry, resulting in a largely intractable optimization problem. We discover, however, an exact mapping of surface minimization onto high-dimensional Feynman diagrams in string theory[5–7], predicting that, with increasing link thickness, a locally tree-like network undergoes a transition into configurations that can no longer be explained by length minimization. Specifically, surface minimization predicts the emergence of trifurcations and branching angles in excellent agreement with the local tree organization of physical networks across a wide range of application domains. Finally, we predict the existence of stable orthogonal sprouts, which are not only prevalent in real networks but also play a key functional role, improving synapse formation in the brain and nutrient access in plants and fungi.

The vascular system and the brain are examples of physical networks that differ from the networks typically studied in network science owing to the tangible nature of their nodes and links, which are made of material resources and constrain their layout. The importance of these material factors has been noted in many disciplines: as early as 1899, Ramón y Cajal suggested that we must consider the laws conserving the 'wire' volume to explain neuronal design[8] and in 1926, Cecil D. Murray applied volume minimization principles to vascular networks, deriving the branching principles known as Murray's law[9]. Today, wiring optimization is used to account for the morphology and the layout of a wide range of physical systems[10,11], from the distributions of neuronal branch sizes[12] and lengths[13] to the morphology of plants[14], the structure[15] and flow[16] in transport networks, the layout of supply networks[17], the wiring of the Internet[18] or the shape of inter-nest trails built by Argentine ants[19] and the design of 3D-printed tissues with functional vasculature[20].

The premise of wiring economy approaches is the optimal wiring hypothesis, which conceptualizes physical networks as a set of connected one-dimensional wires whose total length is minimized[21–23]. The optimal wiring in this case is exactly predicted by the Steiner graph[24–27]. However, the lack of high-quality data on physical networks has limited the systematic testing of the Steiner predictions to single neuron branches[28] and ant tunnels[19] and offered at best mixed evidence of their validity[28,29]. Yet, data availability has substantially improved in the past few years, thanks to advances in microscopy and three-dimensional reconstruction techniques, offering access to the detailed three-dimensional structure of physical networks ranging from high-resolution layouts of brain connectomes[1–3] to vascular networks[4] or the structure of coral trees[30]. Here we take advantage of these experimental advances to explore in a quantitative manner the role of wiring optimization in shaping the local morphology of physical networks. We begin by documenting systematic deviations from both the Steiner predictions[24] and volume optimization[9,28,29], failures that we show to be rooted in the hypothesis that approximates the cost of physical networks as the sum of their link lengths[21–23] or as simple cylinders[28,29]. Indeed, the links of real physical networks are inherently three-dimensional, prompting us to suggest that their true material cost must also consider surface constraints. Building on previous analyses that introduced volumetric constraints[9,28,29], here we successfully account for the local surface morphology, ensuring that, when links intersect, they morph together continuously and smoothly, free of singularities, as dictated by the physicality of their material structure. To achieve this, we map the local tree structure of physical networks into two-dimensional manifolds, arriving at a numerically intractable surface and volume minimization problem. We discover, however,

[1]Department of Physics, Applied Physics, and Astronomy, Rensselaer Polytechnic Institute, Troy, NY, USA. [2]National Institute for Theory and Mathematics in Biology, Northwestern University and The University of Chicago, Chicago, IL, USA. [3]Network Science Institute, Northeastern University, Boston, MA, USA. [4]Department of Physics, Northeastern University, Boston, MA, USA. [5]Department of Mathematics, Bar-Ilan University, Ramat Gan, Israel. [6]The Gonda Multidisciplinary Brain Research Center, Bar-Ilan University, Ramat Gan, Israel. [7]Channing Division of Network Medicine, Department of Medicine, Brigham and Women's Hospital, Harvard Medical School, Boston, MA, USA. [8]Department of Network and Data Science, Central European University, Budapest, Hungary. ✉e-mail: a.barabasi@northeastern.edu

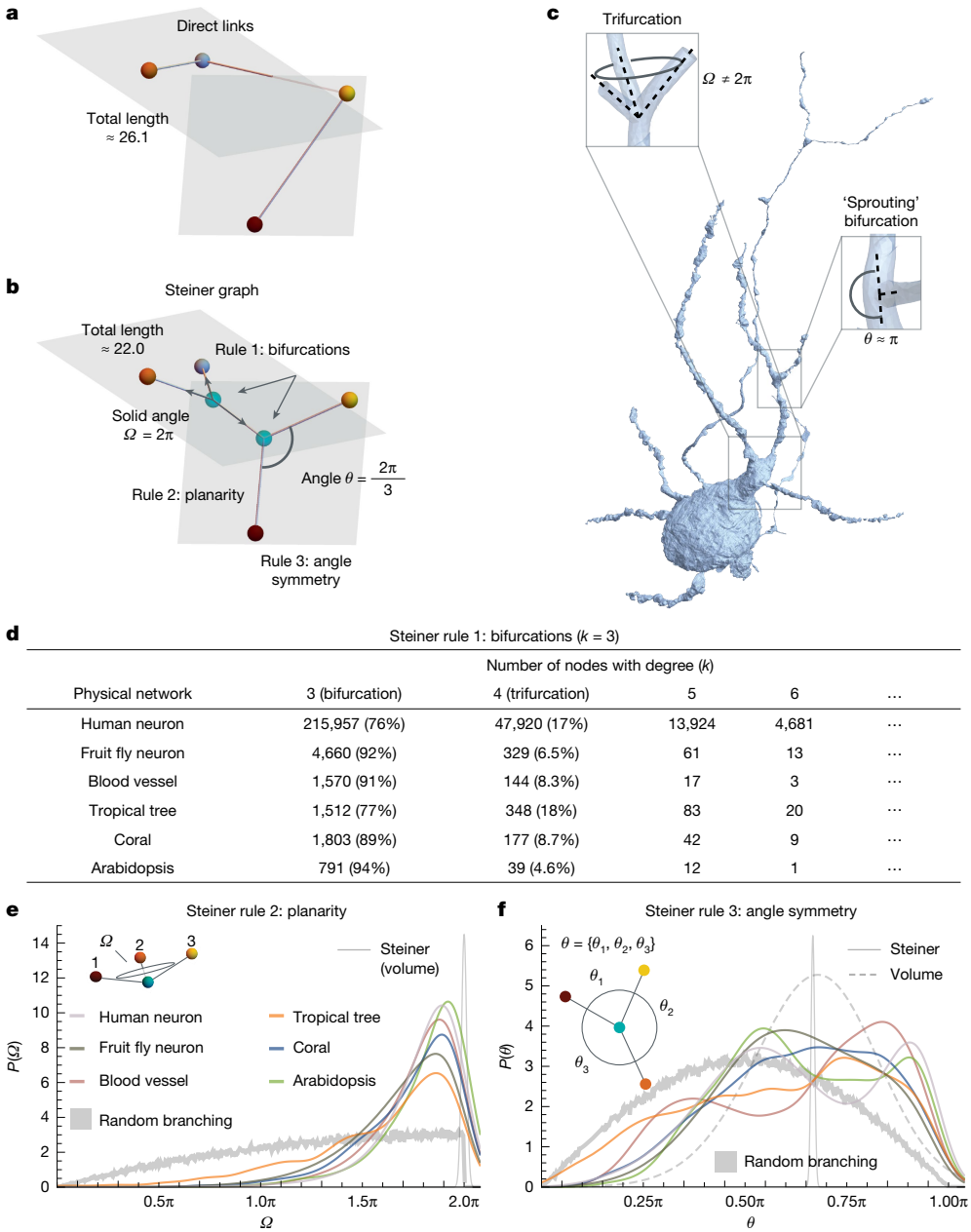

d Steiner rule 1: bifurcations ($k = 3$)

Physical network	Number of nodes with degree (k)				
	3 (bifurcation)	4 (trifurcation)	5	6	…
Human neuron	215,957 (76%)	47,920 (17%)	13,924	4,681	…
Fruit fly neuron	4,660 (92%)	329 (6.5%)	61	13	…
Blood vessel	1,570 (91%)	144 (8.3%)	17	3	…
Tropical tree	1,512 (77%)	348 (18%)	83	20	…
Coral	1,803 (89%)	177 (8.7%)	42	9	…
Arabidopsis	791 (94%)	39 (4.6%)	12	1	…

Fig. 1 | Real physical networks versus length and volume optimization predictions. a, Physical networks aim to connect spatially distributed nodes (coloured) with physical links in three dimensions. If we connect nodes directly, the wiring cost (total link length) is about 26.1. **b**, The Steiner graph minimizes the wire length by permitting intermediate nodes (green), resulting in the total wire length of approximately 22.0. The Steiner graph offers three predictions. Rule 1: all branching instances are bifurcations with degree $k = 3$. Rule 2: bifurcations are all planar, having a solid angle of $\Omega = 2\pi$. Rule 3: the angles between adjacent links are $\theta = 2\pi/3$. Volume optimization, which generalizes links as simple cylinders of varying thickness, preserves rules 1 and 2 and predicts a broader distribution for θ, peaked around $2\pi/3$. **c**, A neuron of the human connectome, demonstrating the violations of the Steiner rules. In the top inset, we highlight a trifurcation ($k = 4$) violating rule 1. We also highlight a non-symmetric branching angle, in which links sprout out perpendicularly (right inset), breaking rule 3. **d**, The percentage of $k = 4$ nodes across our six empirical locally tree-like physical networks. We observe roughly 15% of the nodes violating Steiner rule 1. **e**, The probability density $P(\Omega)$ versus Ω as obtained from all bifurcations ($k = 3$) in our empirical network ensemble (coloured solid lines). The observed density functions are more prone to Steiner rule 2 (thin grey line) than to random branching without optimization (thick grey line). **f**, The probability density $P(\theta)$ versus θ as obtained from all bifurcations (coloured solid lines). Once again, we observe a clear discrepancy from Steiner (thin grey line) and a tendency towards random branching (thick grey line) or volume optimization of cylindrical links with random thickness (dashed grey line).

a formal mapping between surface minimization and high-dimensional Feynman diagrams, which allows us to take advantage of a well-developed string-theoretical toolset[5–7] to predict the basic characteristics of minimal surfaces. We find that surface minimization can not only account for the empirically observed discrepancies from the Steiner predictions but offers testable predictions on the degree distribution and the angle asymmetry of physical networks, which we can falsify, offering a crucial window into the design principles of physical networks.

Steiner graphs

The Steiner graph problem[24] begins with M spatially distributed nodes (Fig. 1a), with the task of connecting these nodes through the

shortest possible links. The key insight of the Steiner solution is that, by adding intermediate nodes to serve as branching points (Fig. 1b), the obtained link length can be shorter than any attempt to connect the nodes directly[24] (Fig. 1a). Although for arbitrary M the Steiner problem is NP-hard, for $M = 4$, we can get an exact solution, resulting in a globally optimal Steiner graph that is characterized by three strict local rules (Fig. 1b). (1) Bifurcation only. All branching instances represent bifurcations, in which a single link splits into two daughter links. Consequently, all intermediate nodes have degree $k = 3$ and higher-degree nodes ($k > 3$) are forbidden. (2) Planarity. At a bifurcation, all three links are embedded in the same plane ($\Omega = 2\pi$). (3) Angle symmetry. All three branches of a bifurcation form the same angle $\theta = 2\pi/3$ with each other.

To test the validity of the local predictions of the Steiner solution, we collected three-dimensional resolved data of six classes of physical networks (Supplementary information Section 1): (1) human neurons[1] (also in Fig. 1c); (2) fruit fly neurons[31]; (3) human vasculature[4]; (4) tropical trees from moist forests[32]; (5) corals of several species[30]; (6) arabidopsis at different growth stages[33]. As wiring optimization relies on the skeleton representations of physical networks, we confirmed that our test of Steiner's prediction is not sensitive to the choice of the particular skeletonization algorithm (Supplementary information Section 1). To examine the validity of rule 1 (bifurcation only), we extracted the degree distribution of each skeletonized network. In agreement with the Steiner principle (an outcome also predicted by volume optimization of simple cylinders[28,29]), we observe a prevalence of $k = 3$ nodes, accounting, for example, for 79% of the nodes in the human neurons and for 94% in arabidopsis. Yet, we also observe a substantial number of trifurcations ($k = 4$) and several even higher degree ($k = 5, 6$) nodes (Fig. 1d), violating the Steiner and volume optimization prediction[34,35]. Note that, because of errors in skeletonizing a physical motif, two closely spaced bifurcations may be mistakenly identified as a trifurcation or, conversely, a trifurcation may be incorrectly perceived as two bifurcations[36]. We therefore verified that the observed high-degree nodes (as demonstrated in Fig. 1c) cannot be attributed to resolution limits (Supplementary information Section 1).

To examine the validity of rule 2 (planarity), which is predicted by both Steiner and volume optimization, we quantified the planarity for each bifurcation ($k = 3$) by measuring the probability $P(\Omega)$ that the three links span a solid angle Ω. We find that, in all of the studied networks, $P(\Omega)$ is strongly peaked at a solid angle that is smaller than the expected $\Omega = 2\pi$, which is necessary (and sufficient) for planarity (Fig. 1e). Finally, to test the validity of rule 3 (angle symmetry), we extracted the pairwise angles ($\theta_1, \theta_2, \theta_3$) between the links at each bifurcation, measuring the probability density $P(\theta)$. As Fig. 1f indicates, none of the six classes of real networks have a peak at the predicted $\theta = 2\pi/3$ but instead the branching angles are broadly distributed, an asymmetry violating the Steiner prediction. Note that $P(\theta)$ predicted by volume optimization is also peaked around $\theta = 2\pi/3$ but it can account for a broader range of branching angles thanks to the fact that links can have varying thickness[28,29].

Taken together, although we see the signature of the Steiner theorem and volume optimization in the prevalence of $k = 3$ nodes, the optimal wiring hypothesis is unable to account for the existence of $k > 3$ nodes, the prevalence of non-planar bifurcations and the lack of $\theta = 2\pi/3$ symmetry, results that question the validity of the optimal wiring hypothesis for physical networks.

Beyond wires—physical networks as manifolds

The Steiner problem relies on the hypothesis that nature aims to minimize the total length of the links, solving an inherently global problem. However, real physical networks have rich local geometries (Fig. 1c), characterized by varying diameters[9] and non-cylindrical surface morphologies. Over the past century, beginning with Murray's 1926 work,

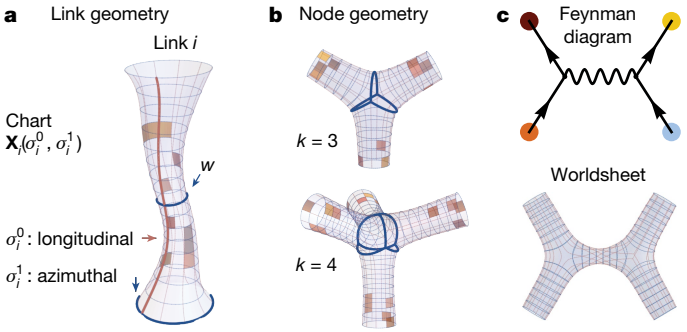

Fig. 2 | Physical network manifold. a, In a physical network, the links are represented by charts, with a manifold morphology $\mathbf{X}_i(\boldsymbol{\sigma}_i)$. Each chart i is described by its local coordinate system $\boldsymbol{\sigma}_i$. The natural parametrization of a surface is provided by the longitudinal (σ_i^0, red) and azimuthal (σ_i^1, blue) coordinates. The minimum circumference around a link is denoted by w, measured along a path in the azimuthal direction. **b**, The intersections between the links define the geometry around the nodes. The local charts must be stretched and expanded to ensure a smooth and continuous patching at their boundaries (blue lines), guaranteeing that $\boldsymbol{\sigma}_i = (\sigma_i^0, \sigma_i^1)$ match perfectly with $\boldsymbol{\sigma}_j = (\sigma_j^0, \sigma_j^1)$ at the i, j intersection. **c**, A Feynman diagram (top) describes the interactions between elementary particles in field theory. In string theory, Feynman diagrams are smooth and continuous manifolds in higher dimensions (bottom), known as a worldsheet, that translate the discrete diagram at the top into the integrable object at the bottom. An exact mapping of the surface minimization problem (equations (1) and (2)) to these higher-dimensional worldsheets allows us to map abstract geometry into a structurally consistent physical network.

researchers have combined geometry-based volume optimization calculations[9,28,29] with algorithmic approximations to identify network configurations that satisfy the inherent system-specific constraints and align with experimental data in specific domains[37–39]. However, these approaches cannot account for either the smoothness of the joints that characterize real physical networks or for the cost associated with deviations from a simple linear or cylindrical solution. Indeed, to account for the true cost of building and maintaining these networks, we must capture the full morphology of a locally tree-like system, which is best described as a manifold $\mathcal{M}(\mathcal{G})$ assigned to the graph $\mathcal{G}$. Formally, a manifold is a series of charts representing local coordinate systems that, when patched together, define a global coordinate system, or an atlas[40]. Previous advances related graphs to discrete manifolds through the use of simplicial complexes, assembled to form an atlas of connected, discrete coordinates[41–43]. Here, however, we aim to build smooth manifolds by formally describing each chart as a continuous surface embedded in three dimensions, whose shape is described by three-dimensional coordinates $\mathbf{X} = (x, y, z)$, in which $x(\boldsymbol{\sigma})$, $y(\boldsymbol{\sigma})$ and $z(\boldsymbol{\sigma})$ are two-variable functions of a local, two-dimensional coordinate system, $\boldsymbol{\sigma} = (\sigma^0, \sigma^1)$ (Fig. 2a). This formalism replaces the total link length in the Steiner graph (Supplementary information Section 2) with the total surface area $S_{\mathcal{M}(\mathcal{G})}$ (Supplementary information Section 3):

$$S_{\mathcal{M}(\mathcal{G})} = \sum_{i=1}^{L} \int \mathrm{d}^2\boldsymbol{\sigma}_i \sqrt{\det \gamma_i}. \tag{1}$$

Here γ_i is given by $\gamma_{i,\alpha\beta} \equiv (\partial \mathbf{X}_i/\partial \sigma_i^{\alpha}) \cdot (\partial \mathbf{X}_i/\partial \sigma_i^{\beta})$ (ref. 40), characterizing the infinitesimal surface area elements of each link i. Hence, equation 1 sums over the surfaces of sleeve-like charts $\mathbf{X}_i(\boldsymbol{\sigma}_i)$ dressed over the links $i = 1, \ldots, L$ of graph $\mathcal{G}$ (Fig. 2). To ensure that the sleeves form a smooth manifold (Supplementary information Section 4) and describe a compact physical object, they must obey several strict conditions: (1) to avoid non-physical cusps when two (or more) sleeves are sewn together, the ends of the sleeves must be perfectly aligned (Fig. 2b);

(2) in principle, surface minimization can collapse a link, predicting that the minimum solution requires a thinning out at mid-point (Supplementary information Section 5). However, many real physical networks must support material flux, which requires a minimum circumference w everywhere, hence surface minimization is also subject to the functional constraint

$$\oint_{\text{circumference}} \mathrm{d}l_i \geq w, \tag{2}$$

in which the arc length is given by $\mathrm{d}l_i^2 = \sum_{\alpha,\beta} \gamma_{i,\alpha\beta} \mathrm{d}\sigma_i^{\alpha} \mathrm{d}\sigma_i^{\beta}$.

We, therefore, arrive at our final optimization problem: given a set of terminals (predetermined nodes), we seek the smooth and continuous surface manifold that links all terminals through finite paths, whose circumference exceeds the predefined threshold w and minimizes the cost $S_{\mathcal{M}(\mathcal{G})}$ (equation (1)). At first glance, this optimization problem is intractable, as we must compare an uncountably infinite set of circumferences, known as non-contractable closed curves[44], ensuring that none of them violate equation (2) while minimizing equation (1). Our key methodological advance is the discovery of a direct equivalence between the network manifold minimization problem defined above and higher-dimensional Feynman diagrams (known as pants decomposition) in string theory[5–7]. The traditional Feynman diagram is a graph $\mathcal{G}$ that views particle trajectories as links and collisions as nodes (Fig. 2c). String (field) theory generalizes Feynman diagrams to two-dimensional surfaces, called the 'worldsheets', which represent the paths that strings sweep through in spacetime[5–7]. The smoothness of this surface guarantees that the path integral does not diverge, making it renormalizable[45], resulting in the Nambu–Goto action[45] that is formally identical to equation (1). The classical solution of the Nambu–Goto action, obtained in the absence of quantum fluctuations but subject to the constraint of equation (2), is exactly the manifold $\mathcal{M}(\mathcal{G})$ we seek. According to Strebel's theorem, in the absence of boundary conditions, this minimal surface is exactly cylindrical. With boundary conditions added, we can simplify equation (2) to a local constraint (Supplementary information Section 5), allowing us to construct local trees with discrete surfaces that are optimized for both smoothness and minimality. Numerically, this is performed by the min-surf-netw package, described in Supplementary information Section 6 and shared on GitHub.

Degree distribution

We start from a symmetric configuration of four terminals, laid out on the corners of a regular tetrahedron (Fig. 3a) and construct the minimal-surface network motif, represented by a tree that links these four nodes, with minimal link circumference w (Fig. 3b). We define the dimensionless weight parameter, $\chi = w/r$, in which r is the distance between the intermediate nodes. In the $\chi \to 0$ limit, we have a quasi-one-dimensional configuration with long and thin links. In this case, the surface minimization predictions converge to the Steiner rules 1–3 (Fig. 1b), linking the four terminal nodes through two intermediate bifurcations with degree $k = 3$ (Fig. 3c,d). Yet, the optimal solution also predicts that, for higher χ (thicker links), the two $k = 3$ nodes gradually approach each other and that, at $\chi \approx 1$, they merge into a single $k = 4$ node, resulting in a trifurcation (Fig. 3e,f). In other words, surface minimization[7] predicts a transition from a Steiner bifurcation to a stable trifurcation at $\chi \approx 1$, an outcome that eluded volume optimization as well[28,29].

To quantify this transition, we use the dimensionless separation $\lambda = l/w$ as an order parameter, in which l is the length of the link between the two $k = 3$ nodes, and using min-surf-netw (Supplementary information Section 6), we numerically generate the connecting minimal surface, allowing us to measure $\lambda(\chi)$ as a function of χ. For small χ, we have $\lambda > 0$, predicting that the two $k = 3$ nodes are separated, in line with the Steiner prediction (Fig. 3g). Yet, at $\chi \approx 0.83$, we observe a sudden drop to $\lambda = 0$, when the one-dimensional Steiner approximation breaks down and instead surface minimization predicts the emergence of a trifurcation ($k = 4$). This transition represents our first key prediction, indicating that the empirically observed $k = 4$ nodes in locally tree-like physical networks represent a stable configuration predicted by local surface optimization.

To generalize our approach, we place the four terminals randomly in a unit cube and run several configurations to extract the probability density $P(\lambda)$. For $\chi = 0$ (corresponding to $w = 0$, which reduces to the Steiner problem), we find that $P(\lambda) \to 0$ for small separation λ (Fig. 3h, grey line), confirming the absence of trifurcations. By contrast, for large χ (for example, $w = 1$), we find that $P(\lambda \to 0)$ does not vanish (Fig. 3h, green line). Rather, we observe a finite probability for trifurcations with $\lambda = 0$ (Supplementary information Section 7). Figure 3h indicates that the density function $P(\lambda)$ offers an empirically falsifiable fingerprint of surface minimization. We therefore divided each physical network into local groups of four connected links and extracted $P(\lambda)$. We find that each locally tree-like network exhibits a non-vanishing $P(\lambda \to 0)$ (Fig. 3i–n, coloured lines), representing a clear deviation from the Steiner prediction (green line) and offering direct evidence that, in real networks, the cost function is not linear in the link length but is better described by surface minimization.

Angle asymmetry

To understand the origin of the observed angle diversity, a violation of rule 3 (Fig. 1f), we assume that each link i is characterized by its unique circumference constraint w_i. Without a loss of generality, we set $w_1 = w_2 = w$ and $w_3 = w'$, and vary the ratio $\rho = w'/w$, to obtain the minimal manifold that connects nodes 1, 2 and 3 (Fig. 4a,b). Although Steiner's solution posits a constant steering angle $\Omega_{1\to2} \approx 0.3\pi$, surface minimization predicts two distinct regimes separated by a threshold value ρ_{th} (Supplementary information Section 7). (1) For $\rho > \rho_{\text{th}}$, we predict the steering angle $\Omega_{1\to2} \approx k(\rho - \rho_{\text{th}})$ (Fig. 4e,f), that is, a linear dependence on ρ (Fig. 4g). This regime can therefore account for the wide range of angles observed in Fig. 1f. (2) For $\rho < \rho_{\text{th}}$, surface minimization makes an unexpected prediction: if links 1 and 2 have comparable diameters, they are expected to form a straight path (that is, continue with solid angle of $\Omega_{1\to2} = 0$), whereas the thinner link 3 is predicted to emerge perpendicularly at $\Omega_{1\to3} \approx \Omega_{2\to3}$, consistent with an orthogonal sprouting behaviour (Fig. 4c,d). Note that a geometric approach predicted as early as 1976 (refs. 28,29) that the branch angles converge to 90° in the $\rho \to 0$ limit (Supplementary information Section 7). By contrast, our framework predicts that the 90° solution is optimal for any $\rho < \rho_{\text{th}}$ (Fig. 4g). Hence, orthogonal sprouts are not singular solutions that emerge only in the $\rho \to 0$ limit[28,29]. Rather, they are stable solutions of surface minimization that remain minimal for a wide range of parameter values and hence they should be not only observable but prevalent in real physical networks.

To test these predictions, we identified all bifurcation motifs in each network in our database and then searched for branches that satisfy $w_1 = w_2 = w$. We then measured $\Omega(\rho) = \Omega_{1\to2}$ as a function of the empirically observed ρ, finding that almost all bifurcations for $\rho < \rho_{\text{th}}$ are sprout-like, characterized by small $\Omega(\rho)$ (Supplementary information Section 7). In Fig. 4i–n, we show the cumulative value of the observed angles in the two regimes, offering evidence that the cumulative $|\int_{\rho}^{\rho_{\text{th}}} \Omega(\rho)\mathrm{d}\rho|$ follows approximately $(\rho_{\text{th}} - \rho)^1$ for $\rho < \rho_{\text{th}}$ and a quadratic behaviour approximately $(\rho - \rho_{\text{th}})^2$ for $\rho > \rho_{\text{th}}$, in line with the predictions of Fig. 4g.

The key outcome of surface minimization is the predicted prevalence of the orthogonal sprouts, expected to emerge each time $\rho < \rho_{\text{th}}$. To falsify this prediction, we ask: are such sprouts really present in physical networks? Note that the excess of sprouts over the expectations of length or volume optimization was already noted in arterial systems as early as 1976 (ref. 29). This abundance remained unanswered and it also remains unclear whether sprouts represent a generic feature

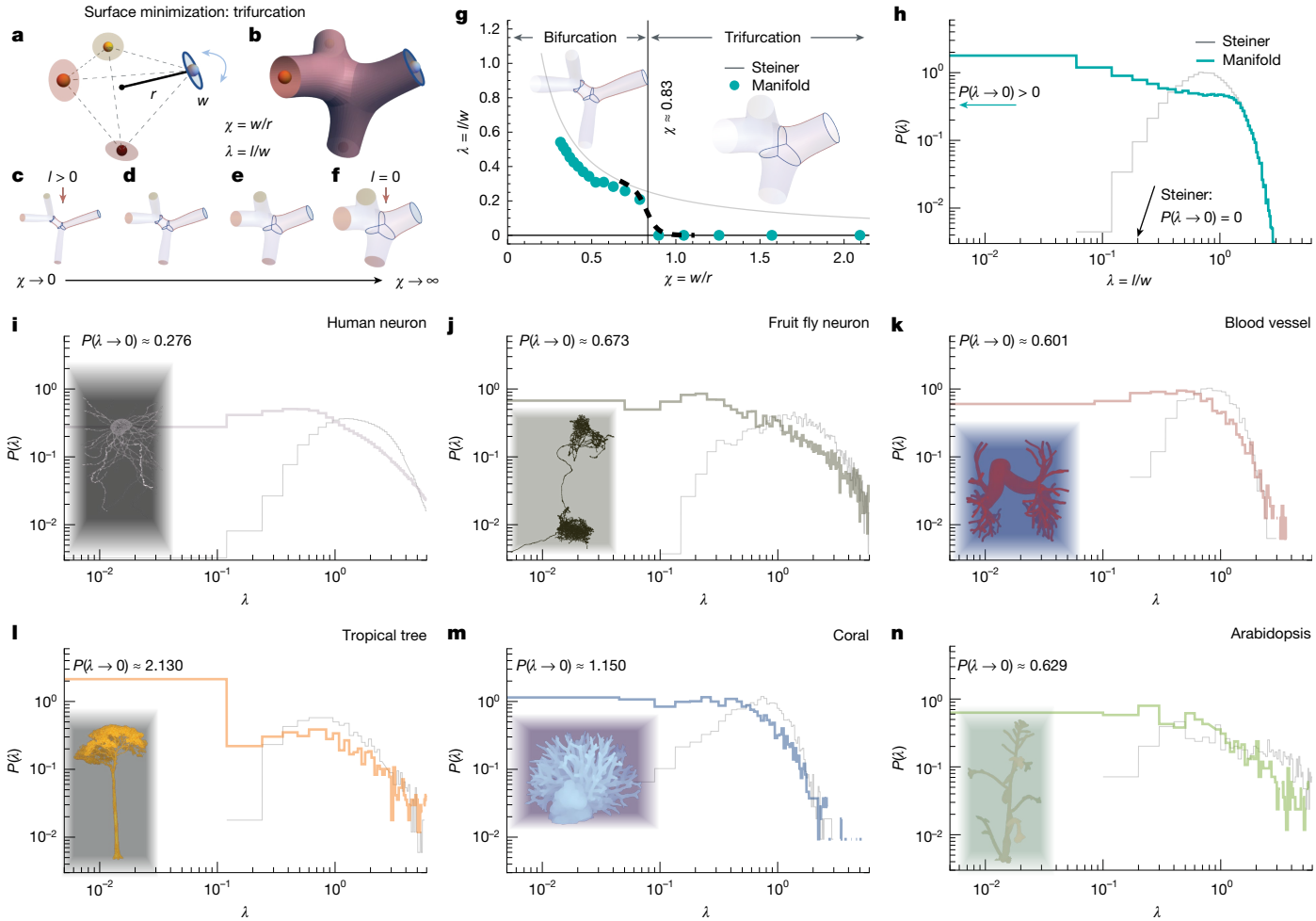

Fig. 3 | Emergence of trifurcations. a, We consider four nodes forming a perfect tetrahedral configuration with spatial length scale r, capturing the radius of the tetrahedron. **b**, We construct a physical network to link these four nodes under surface minimization with circumference constraint w (link thickness). **c**,**d**, When $\chi = w/r \to 0$, the sleeves behave as one-dimensional links and the resulting manifold is well approximated by the Steiner solution, the network featuring two $k = 3$ bifurcations. **e**,**f**, As χ increases, the intermediate link l becomes shorter, until, beyond a certain thickness, the separation parameter $\lambda = l/w \to 0$, indicating that the two intermediate bifurcations unite into a single trifurcation with $k = 4$. **g**, To examine the predicted transition, we plot λ versus χ for the minimal surface (green). For small χ, we have $\lambda > 0$, following a pattern also predicted by Steiner (grey line). This captures the two-bifurcation scenario predicted by length minimization. However, at $\chi \approx 0.83$, we observe a sudden decrease to $\lambda = 0$, capturing the transition from double bifurcations to a single trifurcation. **h**, We examined a series of random four-node configurations within a unit cube and implicitly constructed for each a Steiner graph and a minimal-surface manifold ($w = 1$). We then extracted $P(\lambda)$, capturing the probability density to observe λ. Under Steiner optimization, $P(\lambda)$ vanishes as $\lambda \to 0$ (grey curve), capturing the fact that trifurcations are forbidden. By contrast, for surface minimization (green curve), we have $P(\lambda \to 0) > 0$, describing a finite likelihood to observe trifurcations. **i**–**n**, $P(\lambda)$ versus λ obtained from real physical networks. In each network, we collected all tetrahedral motifs in which the four external nodes are linked through two intermediate nodes and extracted λ between these intermediaries. Compared with Steiner's predictions (grey lines), the empirically observed $P(\lambda)$ (distinct colours) follows the green pattern in **h**, capturing a coexistence of bifurcations ($\lambda > 0$) and trifurcations ($\lambda = 0$), as predicted by surface minimization.

across all physical networks or are unique to blood vessels. To address this, we first identified all bifurcations with $w_1 \approx w_2$ in blood vessels, confirming that, in 25.6% of the cases, the third branch, independent of ρ, is perpendicular to the main branches, representing an abundant sprouting behaviour. Yet, we find that sprouts are not limited to the circulatory system but are present in all studied networks, representing 12.9% of the $w_1 \approx w_2$ cases in the tropical trees, 52.8% in corals, 11.2% in arabidopsis, 13.8% in the fruit fly neurons and 18.4% in the human neurons. Most importantly, some systems have learned to turn sprout behaviour to their advantage, assigning it a functional role. Indeed, in the human connectome, we identified 4,003 sprouts, finding that 3,911 of these (98%) end with a synapse (Fig. 4h). In other words, neuronal systems have adapted to rely on surface minimization by using orthogonal sprouts as dendritic spines that allow them to form synapses with nearby neurons with minimal material cost. Similarly, roots in plants[46] and hyphae branches in fungi[47] are known to sprout perpendicularly, allowing plants and fungi to explore a larger volume of soil for water and nutrients with minimal material expenditure.

The predicted relation between $\Omega(\rho)$ and ρ in Fig. 4g leads to further falsifiable predictions for the $P(\Omega)$ angle distributions, conditioned on the empirically observed ρ values. In the sprouting regime ($\rho < \rho_{th}$), we predict $\Omega = 0$, independent of ρ, hence we anticipate a sharp peak of $P(\Omega)$ at $\Omega = 0$, in agreement with the empirical data (left side, sprouting regime in Fig. 5a–f). In the branching regime ($\rho > \rho_{th}$), however, $P(\Omega)$ is predicted to exhibit a broad distribution with high variance, rooted in the linear behaviour of Fig. 4g. The empirical data support this prediction as well (right side, branching regime in Fig. 5a–f). By comparison, the Steiner prediction posits a sharp peak of $P(\Omega)$ independent of ρ (thin grey lines in both sprouting and branching regimes in Fig. 5a–f).

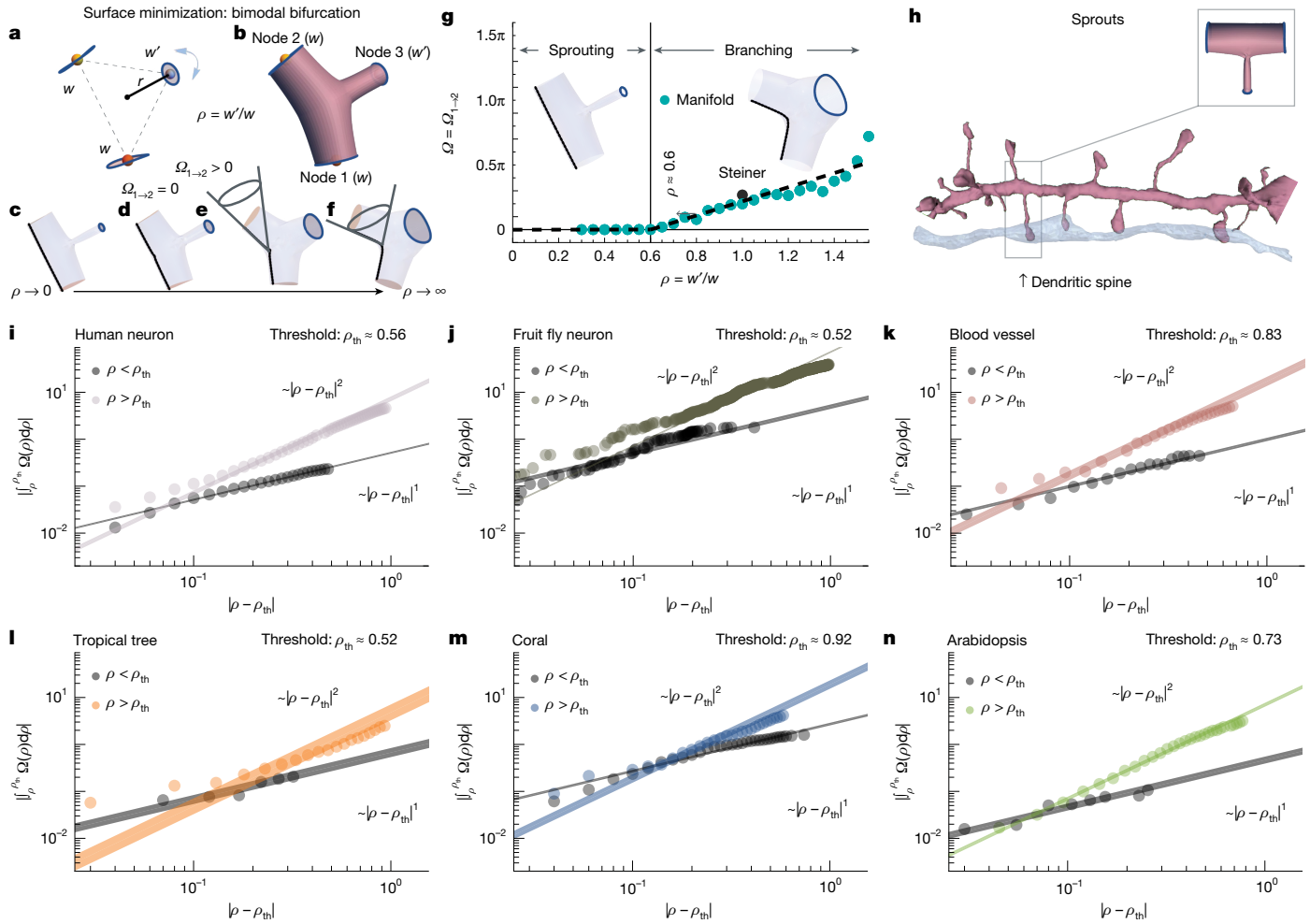

Fig. 4 | Branching versus sprouting bifurcations. a, We start from a triangular node configuration, with $w_1 = w_2 = w$ and $w_3 = w'$. **b**, We construct the minimal-surface manifold connecting the three nodes. **c**,**d**, For small $\rho = w'/w$, the link of node 3 is thin and the optimal manifold favours a sprouting structure: nodes 1 and 2 linked through a straight line and node 3 by means of a perpendicular link. **e**,**f**, For large ρ, we find a linear relation between ρ and the three-dimensional steering angle, $\Omega_{1\to2}$, related to the branching angle θ (Fig. 1f) through $\Omega_{1\to2} = 4\pi\sin^2((\pi - \theta)/4)$. As ρ increases, the bifurcation point approaches the triangle centre and the bifurcation gradually resembles a symmetric branching. **g**, $\Omega_{1\to2}$ versus ρ. We observe a transition from sprouting ($\Omega = 0$) to branching ($\Omega > 0$) at $\rho \approx 0.6$. The symmetric branching observed by Steiner appears near $\rho = 1$. **h**, In the human connectome, 92% of the observed sprouts end on synapses, suggesting that neuronal systems use surface minimization to form direct synaptic connections to adjacent neurons with minimal material cost. **i**–**n**, According to **g**, cumulative $\left|\int_{\rho}^{\rho_{th}} \Omega(\rho)\mathrm{d}\rho\right|$ should follow approximately $(\rho_{th} - \rho)^1$ for $\rho < \rho_{th}$ and approximately $(\rho - \rho_{th})^2$ for $\rho > \rho_{th}$, predictions closely followed by real physical networks. Band thickness represents one standard error of the fitting.

Discussion

The three-dimensional layout of physical networks is subject to several, often evolutionary-induced, constraints. For example, brain wiring is governed by developmental programs[48] and locally guided by a complex inventory of chemoattractants and repellents that govern the journey of an individual neuron across the brain. Similarly, the vascular system must transport nutrients to all cells and is subject to several optimization goals, from flow efficiency to material cost[49]. Given the diversity of the processes that govern the development of physical networks, we would expect that minimization principles are ultimately overwritten by global and functional needs[50,51]. By contrast, here we find that physical networks observed in a wide range of systems follow common quantifiable morphological branching characteristics that are well predicted by a local surface minimization process. The robustness of our results across several systems indicates that cost minimization is a stereotypical principle that is not overwritten by functional or global need; rather, development and selection probably rely on these local minimization processes to add function to a network. As local optimization does not necessarily dictate the global optimum[28], functional demands may exert greater influence at larger scales[20,38]. For example, we find that wiring optimization fails to correctly predict the total length of physical networks, which are, on average, 25% longer than Steiner's prediction across all six datasets (Supplementary information Section 8).

More empirical studies are needed to validate surface minimization predictions across more complex network structures[52]. Indeed, although here we focused on the universal branching characteristics of locally tree-like structures, construction of larger-scale structures could reveal whether specific network types exhibit unique geometrical adaptations, such as varying link thickness and curvature, owing to the unique functional pressures of the networks, such as flow conservation in vascular systems[9] or neuron placement constraints[48]. These features are beyond the scope of our present surface minimization framework, which predicts straight, uniform cylinders far from the branching points. Furthermore, loops—which we find to be absent in our datasets (Supplementary information Section 8) but ubiquitous in engineered networks such as traffic and power grids—represent a departure from simple wiring efficiency, hence requiring an extended analytical framework. Such advances will

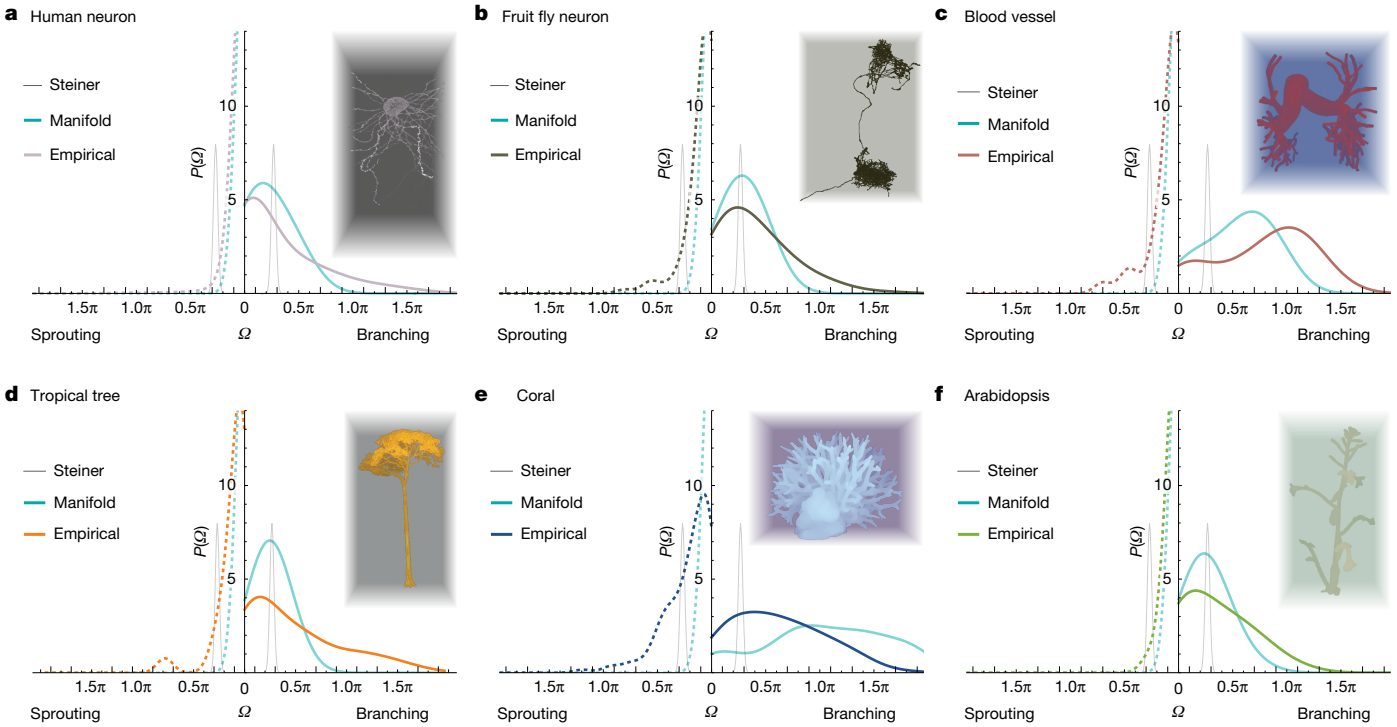

Fig. 5 | Sprouting in physical networks. We predicted and measured the branching angle distribution across six physical networks. **a**–**f**, The relation of $\Omega_{1\to2}$ versus ρ in Fig. 4 predicts distinct distributions $P(\Omega)$ based on the observed ρ values in the sprouting (dashed lines) and branching (solid lines) regimes. Both distributions align with our predictions (green), violating the Steiner predictions (grey).

open avenues to integrate crowding[10,53], knotting[11,54] or bundling[55] of physical links, exploring their influence on the global layout. Such extensions could offer further insights into how networks balance efficiency with functional demands[56] and help us understand how a global and functional organization can emerge from local processes. They may also offer insight into differences between classes of physical networks, helping us understand which features are governed by optimization principles and which require further functional considerations.

Future work could also compare the predicted manifold geometries directly to the observed geometric features, such as surface geodesics, curvatures and other fine details, helping reveal the degree to which the surface minimization model reproduces the observed local geometry beyond skeletons. Indeed, we find that trifurcation junctions are consistently smooth and that their shapes strongly prefer symmetric morphology, features predicted by surface minimization (Supplementary information Section 9). This validation at the level of fine-grained geometry reinforces the empirical foundation of our framework and opens avenues for more detailed comparison with the predictions.

Physical networks in the three-dimensional Euclidean space can be described as either two-dimensional manifolds $\mathcal{M}(\mathcal{G})$ subject to surface minimization or three-dimensional objects subject to volume optimization. Although in vascular networks the material investment is limited to the surface area of the blood vessels, for neurons, corals and trees, an accurate accounting of the material cost must also consider the volume of the branches. The existing literature on volume optimization assumes cylindrical links[28,29] and fails to account for non-trivial topologies emerging at the intersections. As the min-surf-netw algorithm exploits the string-theoretic solution, it is limited to surface minimization. Yet, the two problems are not independent: our numerical simulations indicate that, for the branching processes, suboptimal surfaces also increase the volume, suggesting that the minimal surfaces correspond to close-to-optimal volumes as well (Supplementary information Section 10). However, further work is needed to understand whether a self-consistent volume optimization could offer new solutions and morphologies that are not predicted by our present framework, hence can further enrich our understanding of physical networks.

Online content

Any methods, additional references, Nature Portfolio reporting summaries, source data, extended data, supplementary information, acknowledgements, peer review information; details of author contributions and competing interests; and statements of data and code availability are available at https://doi.org/10.1038/s41586-025-09784-4.

1. Shapson-Coe, A. et al. A petavoxel fragment of human cerebral cortex reconstructed at nanoscale resolution. *Science* **384**, eadk4858 (2024).
2. The MICrONS Consortium. Functional connectomics spanning multiple areas of mouse visual cortex. *Nature* **640**, 435–447 (2025).
3. Winding, M. et al. The connectome of an insect brain. *Science* **379**, eadd9330 (2023).
4. Wilson, N. M., Ortiz, A. K. & Johnson, A. B. The vascular model repository: a public resource of medical imaging data and blood flow simulation results. *J. Med. Devices* **7**, 040923 (2013).
5. Witten, E. Non-commutative geometry and string field theory. *Nucl. Phys. B* **268**, 253–294 (1986).
6. Carlip, S. Quadratic differentials and closed string vertices. *Phys. Lett. B* **214**, 187–192 (1988).
7. Saadi, M. & Zwiebach, B. Closed string field theory from polyhedra. *Ann. Phys.* **192**, 213–227 (1989).
8. Cajal, S. R. Y., Azoulay, D. L., Swanson, N. & Swanson, L. W. *Histology Of The Nervous System: Of Man And Vertebrates* (Oxford Univ. Press, 1995).
9. Murray, C. D. The physiological principle of minimum work. *Proc. Natl Acad. Sci. USA* **12**, 207–214 (1926).
10. Dehmamy, N., Milanlouei, S. & Barabási, A.-L. A structural transition in physical networks. *Nature* **563**, 676–680 (2018).
11. Liu, Y., Dehmamy, N. & Barabási, A.-L. Isotopy and energy of physical networks. *Nat. Phys.* **17**, 216–222 (2021).
12. Budd, J. M. L. et al. Neocortical axon arbors trade-off material and conduction delay conservation. *PLoS Comput. Biol.* **6**, e1000711 (2010).
13. Markov, N. T. et al. Cortical high-density counterstream architectures. *Science* **342**, 1238406 (2013).
14. Wang, Z., Zhao, M. & Yu, Q.-X. Modeling of branching structures of plants. *J. Theor. Biol.* **209**, 383–394 (2001).
15. Durand, M. Architecture of optimal transport networks. *Phys. Rev. E* **73**, 016116 (2006).

16. Bontorin, S., Cencetti, G., Gallotti, R., Lepri, B. & De Domenico, M. Emergence of complex network topologies from flow-weighted optimization of network efficiency. *Phys. Rev. X* **14**, 021050 (2024).
17. Banavar, J. R., Maritan, A. & Rinaldo, A. Size and form in efficient transportation networks. *Nature* **399**, 130–132 (1999).
18. D'Souza, R. M., Borgs, C., Chayes, J. T., Berger, N. & Kleinberg, R. D. Emergence of tempered preferential attachment from optimization. *Proc. Natl Acad. Sci. USA* **104**, 6112–6117 (2007).
19. Latty, T. et al. Structure and formation of ant transportation networks. *J. R. Soc. Interface* **8**, 1298–1306 (2011).
20. Sexton, Z. A. et al. Rapid model-guided design of organ-scale synthetic vasculature for biomanufacturing. *Science* **388**, 1198–1204 (2025).
21. Chklovskii, D. & Stevens, C. Wiring optimization in the brain. In *Advances in Neural Information Processing Systems 12: Proc. 1999 Conference* 103–107 (MIT Press, 1999).
22. Chklovskii, D. B., Schikorski, T. & Stevens, C. F. Wiring optimization in cortical circuits. *Neuron* **34**, 341–347 (2002).
23. Kim, Y., Sinclair, R., Chindapol, N., Kaandorp, J. A. & Schutter, E. D. Geometric theory predicts bifurcations in minimal wiring cost trees in biology are flat. *PLoS Comput. Biol.* **8**, e1002474 (2012).
24. Hwang, F. K., Richards, D. S. & Winter, P. *The Steiner Tree Problem* 1st edn (Elsevier, 1992).
25. Rosenthal, A. Computing the reliability of complex networks. *SIAM J. Appl. Math.* **32**, 384–393 (1977).
26. Winter, P. Steiner problem in networks: a survey. *Networks* **17**, 129–167 (1987).
27. Amirghasemi, M. et al. in *Frontiers in Nature-Inspired Industrial Optimization* 1st edn (eds Khosravy, M., Gupta, N. & Patel, N.) 33–48 (Springer, 2022).
28. Cherniak, C. Local optimization of neuron arbors. *Biol. Cybern.* **66**, 503–510 (1992).
29. Zamir, M. Optimality principles in arterial branching. *J. Theor. Biol.* **62**, 227–251 (1976).
30. Corals – 3D digitization. https://3d.si.edu/corals.
31. Scheffer, L. K. et al. A connectome and analysis of the adult *Drosophila* central brain. *eLife* **9**, e57443 (2020).
32. Gonzalez de Tanago, J. et al. Estimation of above-ground biomass of large tropical trees with terrestrial LiDAR. *Methods Ecol. Evol.* **9**, 223–234 (2018).
33. Pan, H., Hétroy-Wheeler, F., Charlaix, J. & Colliaux, D. ARABIDOPSIS 3D+T dataset. *Zenodo* https://doi.org/10.5281/zenodo.5205561 (2021).
34. Percheron, G. Quantitative analysis of dendritic branching. I. Simple formulae for the quantitative analysis of dendritic branching. *Neurosci. Lett.* **14**, 287–293 (1979).
35. Percheron, G. Quantitative analysis of dendritic branching. II. Fundamental dendritic numbers as a tool for the study of neuronal groups. *Neurosci. Lett.* **14**, 295–302 (1979).
36. Miyawaki, S., Tawhai, M. H., Hoffman, E. A., Wenzel, S. E. & Lin, C.-L. Automatic construction of subject-specific human airway geometry including trifurcations based on a CT-segmented airway skeleton and surface. *Biomech. Model. Mechanobiol.* **16**, 583–596 (2017).
37. Schreiner, W. & Buxbaum, P. Computer-optimization of vascular trees. *IEEE Trans. Biomed. Eng.* **40**, 482–491 (1993).
38. Jessen, E., Steinbach, M. C., Debbaut, C. & Schillinger, D. Rigorous mathematical optimization of synthetic hepatic vascular trees. *J. R. Soc. Interface* **19**, 20220087 (2022).
39. Keelan, J., Chung, E. M. L. & Hague, J. P. Simulated annealing approach to vascular structure with application to the coronary arteries. *R. Soc. Open Sci.* **3**, 150431 (2016).
40. Bobenko, A. I., Sullivan, J. M., Schröder, P. & Ziegler, G. M. (eds) *Discrete Differential Geometry* (Birkhäuser, 2008).
41. Bianconi, G. & Rahmede, C. Complex quantum network manifolds in dimension $d > 2$ are scale-free. *Sci. Rep.* **5**, 13979 (2015).
42. Bianconi, G., Rahmede, C. & Wu, Z. Complex quantum network geometries: evolution and phase transitions. *Phys. Rev. E* **92**, 022815 (2015).
43. Bianconi, G. & Rahmede, C. Network geometry with flavor: from complexity to quantum geometry. *Phys. Rev. E* **93**, 032315 (2016).
44. Gromov, M. *Partial Differential Relations* 1st edn (Springer, 1986).
45. Tong, D. Lectures on string theory. *University of Cambridge* http://www.damtp.cam.ac.uk/user/tong/string.html (2009).
46. Lynch, J. P. Steep, cheap and deep: an ideotype to optimize water and n acquisition by maize root systems. *Ann. Bot.* **112**, 347–357 (2013).
47. Harris, S. D. Branching of fungal hyphae: regulation, mechanisms and comparison with other branching systems. *Mycologia* **100**, 823–832 (2008).
48. Barabási, D. L. & Barabási, A.-L. A genetic model of the connectome. *Neuron* **105**, 435–445 (2020).
49. West, G. B., Brown, J. H. & Enquist, B. J. A general model for the origin of allometric scaling laws in biology. *Science* **276**, 122–126 (1997).
50. Thompson, D. W. *On Growth and Form* (Cambridge Univ. Press, 1992).
51. West, G. *Scale: The Universal Laws of Growth, Innovation, Sustainability, and the Pace of Life in Organisms, Cities, Economies, and Companies* (Penguin Press, 2017).
52. Boccaletti, S., Latora, V., Moreno, Y., Chavez, M. & Hwang, D. U. Complex networks: structure and dynamics. *Phys. Rep.* **424**, 175–308 (2006).
53. Pósfai, M. et al. Impact of physicality on network structure. *Nat. Phys.* **20**, 142–149 (2024).
54. Glover, C. & Barabási, A.-L. Measuring entanglement in physical networks. *Phys. Rev. Lett.* **133**, 077401 (2024).
55. Bonamassa, I. et al. Logarithmic kinetics and bundling in physical networks. Preprint at https://arxiv.org/abs/2401.02579 (2024).
56. Cimini, G. et al. The statistical physics of real-world networks. *Nat. Rev. Phys.* **1**, 58–71 (2019).

Data availability

The dataset is available at https://physical.network.

Code availability

The code used for this manuscript is available at https://github.com/Barabasi-Lab/min-surf-netw.

Acknowledgements We are grateful to U. H. Danielsson and F. Ruehle for helpful discussions on the string theory approach. A.-L.B. was partially supported by the NSF award no. 2243104 - COMPASS and by the European Union's Horizon 2020 research and innovation programme no. 810115 - DYNASNET. B.B. was supported by the Israel Science Foundation grant no. 499/19, the Israel-China ISF-NSFC joint research programme grant no. 3552/21, and by the VATAT grant for data science research.

Author contributions All authors contributed to the research. X.M. and A.-L.B. conceived the research. X.M., B.P. and C.B. collected and cleaned the data. X.M. and B.P. analysed the data. X.M. conducted theoretical analysis, designed the algorithm and performed the simulation. B.B., X.M. and A.-L.B. wrote the manuscript. X.M., C.B. and A.-L.B. reviewed and edited the manuscript.

Competing interests A.-L.B. is the scientific founder of Scipher Medicine, Inc., which applies network medicine to biomarker development. The other authors declare no competing interests.

Additional information

Supplementary information The online version contains supplementary material available at https://doi.org/10.1038/s41586-025-09784-4.

Correspondence and requests for materials should be addressed to Albert-László Barabási.

Peer review information *Nature* thanks Bernat Corominas-Murtra, Shakti N. Menon and the other, anonymous, reviewer(s) for their contribution to the peer review of this work.